Linear-Quadratic-Regulator Pointing Control System for a High-Altitude Balloon Payload

John E. White* and Jerry R. Etter†
Sandia National Laboratories, Albuquerque, New Mexico 87185

A linear-quadratic-regulator (LQR) synthesis technique is employed to produce the azimuth and elevation angle controllers for the pointing of a research balloon science payload. The use of LQR synthesis is motivated by the multiple-input/multiple-output nature of the azimuth pointing problem. A controllable state space that is compatible with the LQR synthesis procedure and which produces a controller structure that ensures zero steady-state tracking is determined for each controller. Time responses and a singular value analysis are used to analytically evaluate the performance and robustness of the controllers.

I. Introduction

THIS paper is concerned with the development of a linear-quadratic-regulator (LQR) control system design that is capable of providing accurate pointing for the science payload of a NASA/AT&T Bell Labs/Sandia Labs high-altitude helium research balloon. The payload package resides within the balloon gondola which is integrated with a helium balloon, a gondola recovery parachute, and a ballast hopper system. The assembled system is shown schematically in Fig. 1, and approximate physical data are given in Table 1. The objective of the pointing control system is to provide azimuth angle control of the gondola via the decoupler motor and flywheel, and elevation angle control of the payload package with dual elevation motors. The azimuth angle control problem is complicated by the dynamic coupling between the balloon/recovery parachute and the gondola/ballast hopper via the decoupler motor. The azimuth axis control objective is to use the decoupler motor to isolate the balloon dynamics from those of the gondola while accelerating or decelerating the flywheel about a constant angular velocity to provide precise gondola pointing. Large angle reorientations are to be accomplished via a coordinated use of both the flywheel and decoupler. The elevation control objective is more straightforward in that the elevation angle of the science package mounted within the gondola is controlled directly via the dual elevation drive motors.

The balloon assembly shown in Fig. 1 is intended to provide improved pointing accuracy for balloon science payloads, which are typically gamma ray astronomy experiments. This balloon configuration flew with success on two occasions in 1988 with a NASA Goddard Spaceflight Center designed pointing control system. Sandia Labs and Bell Labs have also been involved with an earlier balloon configuration,[1] which has flown several times since the first flight in 1975. The payload package of this design is mounted within the gondola with elevation and azimuth motors driving the payload relative to the gondola. The balloon and the gondola are connected via a cable suspension and recovery parachute similar to that of the balloon assembly of Fig. 1, but without the decoupler motor. The arrangement of Fig. 1 includes two unique features to provide improved accuracy in azimuth pointing: 1) a decoupler motor for isolating the payload/gondola from the balloon and 2) a flywheel for reducing the effect of friction nonlinearities on small pointing corrections. The intent of this paper is to evaluate the use of LQR synthesis to accomplish these control objectives.

The LQR pointing control system for the balloon assembly of Fig. 1 consists of three control loops, two of which are coupled because of the dynamic interaction that exists between the balloon and the payload gondola. The operator commanded variables are elevation angle, azimuth angle, and the constant flywheel speed. The dynamic coupling between the

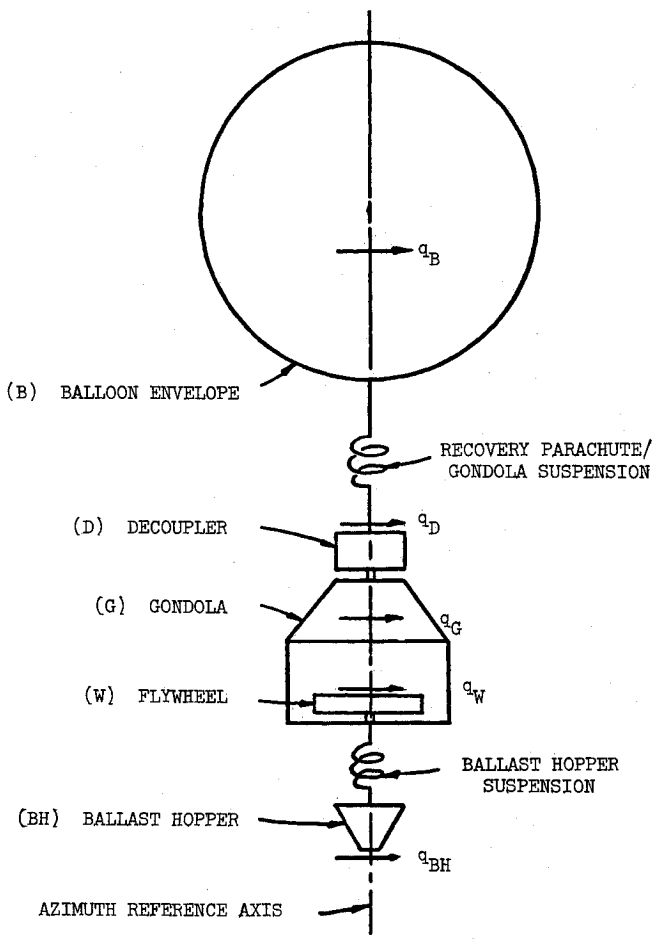

Fig. 1 Balloon assembly schematic.

Presented as Paper 88-4109 at the AIAA Guidance, Navigation, and Control Conference, Minneapolis, MN, Aug. 15-17, 1988; received Oct. 6, 1988; revision received Feb. 15, 1989.

*Senior Member of Technical Staff. Member AIAA.
†Senior Member of Technical Staff.

Table 1 Approximate balloon physical properties

Weights, lb_m:	gondola 2500, payload 2000, ballast 1000
Azimuth axis inertia, $lb_m ft^2$:	gondola 20090.28 flywheel 260.42
Elevation axis inertia, $lb_m ft^2$:	payload 2798.61
Friction coefficients, $lb_f ft$ s:	decoupler 0.05 flywheel 0.05 elevation 0.05
Motor constants, $lb_f ft/A$:	decoupler 0.31 flywheel 0.996 elevation 112.65
Back emf constants, V/rad/s:	decoupler 0.42 flywheel 1.36 elevation 0.42
Winding inductances, H:	decoupler 0.0026 flywheel 0.005 elevation 0.0026
Winding resistances, Ω:	decoupler 1.23 flywheel 1.55 elevation1.23

azimuth angle and the flywheel speed control loops must be accounted for in the control system design. The elevation axis pointing of the science package is assumed for control system design purposes to be dynamically uncoupled from the azimuth axis behavior so that the elevation angle control loop can be independently designed. The sensor package that provides the control system feedbacks includes a magnetometer for the measurement of azimuth and elevation angles, rate gyros for the measurement of rotation rates about the azimuth and elevation axes, and a tachometer for the measurement of flywheel speed. All of the control motors are driven by variable-voltage amplifiers which are commanded by the voltages output from the control laws.

Because of the coupled nature of the balloon azimuth angle pointing control problem, an LQR synthesis technique[2,3] is pursued. LQR methodology is directly applicable to multiple-input/multiple-output (MIMO) problems such as that encountered with the balloon azimuth angle controller and inherently provides the proper loop interconnections. LQR synthesis is also applicable to single-input/single-output (SISO) problems and is used here to design the balloon elevation angle controller and a backup azimuth angle controller. The structure of the LQR SISO compensators is similar to a structure that might be obtained via a classical approach. The MIMO compensator is less easily designed by classical synthesis techniques. While a classical approach to MIMO control problems is usually possible, the selection of the interconnections and individual gains generally complicates the design process and may produce a controller with poorer performance than that obtained by the relatively straightforward, albeit careful, use of LQR synthesis.

As discussed in Refs. 2 and 3, the primary control design consideration is the choice of the state space upon which LQR synthesis is to be applied. The choice of state space in LQR is tantamount to the choice of compensator structure in classical SISO controller design.[2] Hence, the compensator structure for LQR synthesis can be designed or modified by the appropriate choice of the state space. The chosen state space must be controllable and must not have input command dependent system parameters, and all of the states and controls must be zero in steady state. A state space so formed has a well-behaved infinite time quadratic performance index and is suitable for LQR synthesis. The state space should also ensure zero steady-state errors even in the presence of parameter and model uncertainty. This occurs quite naturally when the methodology of Refs. 2 and 3 is implemented because of the resulting integral compensation. The balloon LQR state spaces are formulated to meet the preceding requirements so as to track step commands in each of the controlled variables.

The state and control weighting matrices in the LQR performance index are to be set so that the system transient response characteristics and pointing accuracies are consistent with the requirements of the scientific payload to be flown. Particular attention must be given to the azimuth angle controller weighting matrices such that the balloon and gondola are effectively decoupled so that the flywheel can accelerate/decelerate about a constant angular velocity to provide precise accuracy in azimuth pointing. The robustness of the resulting compensation must also be considered. Full state feedback is required to ensure the LQR gain and phase margin results of Refs. 4–6. In the case of the balloon azimuth and elevation angle control system design to be discussed, all of the required states are measured. However, the guaranteed LQR robustness results of Refs. 4–6 also require that the controls be equally weighted in the performance index. In the case of the azimuth angle controller, simulation studies indicate that the performance of the system is improved with unequal weights on the controls. A singular value analysis is employed to evaluate stability margins and parameter sensitivity, whereas transient responses are used to evaluate the time domain performance of the controllers.

II. System Dynamics

A. Nonlinear Dynamics

This section derives simplified nonlinear equations of motion for the balloon system. The azimuth and elevation dynamics are assumed to be uncoupled, which implies that the gondola hangs directly beneath the balloon without pendulous swinging. This simplification also ignores the very small amount of gyroscopic coupling between the axes due to the flywheel angular momentum. The nonlinear effects due to the transition of the elevation and decoupler motors from a static to a kinetic friction coefficient are also omitted, although the pointing accuracy attainable by the elevation and decoupler alone (backup operating mode) control loops will ultimately be limited by this nonlinearity. These simplifications are reasonable for a model constructed for preliminary control system evaluation.

The balloon/gondola assembly is shown schematically in Fig. 1. The system model comprises the rigid bodies B, D, G, W, and BH, which are free to rotate about the azimuthal reference axis. The orientations of the respective bodies are described by the generalized coordinates q_B, q_D, q_G, q_W, and q_{BH}. Body B represents the balloon envelope and supports the gondola assembly, which consists of the decoupler motor D, the gondola G, the flywheel W, and the ballast hopper BH. Each of these bodies has a moment of inertia about the reference axis designated by I_i where the subscript i is replaced by B, D, G, W, or BH depending on which body is under consideration. Bodies D, G, and W are connected to each other by means of bearings, whereas the pairs of (B,D) and (G,BH) are connected together by cable suspensions. The cable suspensions are assumed to behave as torsional springs. For small relative rotations (a good assumption here), between B and D, and G and BH, the torsional spring torques can be expressed as

$$T_{BD} = k_{BD} \sin(q_D - q_B) \tag{1}$$

$$T_{GBH} = k_{GBH} \sin(q_{BH} - q_G) \tag{2}$$

The sine functions in Eqs. (1) and (2) are required because of the nature of the cable suspensions. T_D and T_W are the control torques applied to the system by d.c. motors located at the decoupler and the flywheel. There are also frictional torques produced by the relative rotations of the bodies. These torques arise from the bearing frictions of the decoupler and flywheel motors. The bearing friction torques are proportional to the

relative speed between D and G, and between G and W. These torques are

$$T_{DG} = \mu_D(\dot{q}_G - \dot{q}_D) \tag{3}$$

$$T_{GW} = \mu_W(\dot{q}_W - \dot{q}_G) \tag{4}$$

The various quantifiable torques acting on the balloon/gondola system are shown in Fig. 2. Aerodynamic friction torques have been neglected, since the balloon will generally operate at altitudes where the atmospheric density is minimal. Disturbance torques (such as wind disturbances) are also not included in the model.

The nonlinear equations of motion about the azimuthal axis are obtained by summing the torques acting on each body independently and applying

$$\Sigma T = I_i \ddot{q}_i \tag{5}$$

where i is to be replaced by B, D, G, W, or BH. The application of Eq. (5) to each of the respective elements of the balloon/gondola assembly produces

$$k_{BD}\sin(q_D - q_B) = I_B\ddot{q}_B \tag{6}$$

$$T_D - k_{BD}\sin(q_D - q_B) + \mu_D(\dot{q}_G - \dot{q}_D) = I_D\ddot{q}_D \tag{7}$$

$$-T_D - T_W + k_{GBH}\sin(q_{BH} - q_G) - \mu_D(\dot{q}_G - \dot{q}_D) + \mu_W(\dot{q}_W - \dot{q}_G) = I_G\ddot{q}_G \tag{8}$$

$$T_W - \mu_W(\dot{q}_W - \dot{q}_G) = I_W\ddot{q}_W \tag{9}$$

$$-k_{GBH}\sin(q_{BH} - q_G) = I_{BH}\ddot{q}_{BH} \tag{10}$$

These equations of motion can be rewritten more conveniently in terms of the variables defined by $\sigma = q_D - q_B$, $\delta = q_G - q_D$, $\beta = q_{BH} - q_G$, $\psi = q_G$, and $\theta = q_W$. If the preceding equations of motion are combined in terms of these variables, the nonlinear equations of azimuthal motion become

$$\dot{\sigma} = \int\ddot{\sigma}\,dt \tag{11}$$

$$\ddot{\sigma} = -k_{BD}(1/I_B + 1/I_D)\sin(\sigma) + (\mu_D/I_D)\dot{\delta} + (1/I_D)T_D \tag{12}$$

$$\ddot{\delta} = (k_{BD}/I_D)\sin(\sigma) - \mu_D(1/I_D + 1/I_G)\dot{\delta} + (k_{GBH}/I_G)\sin(\beta) - (\mu_W/I_G)\dot{\psi} + (\mu_W/I_G)\dot{\theta} - k_D(1/I_G + 1/I_D)T_D - (1/I_G)T_w \tag{13}$$

$$\dot{\beta} = \int\ddot{\beta}\,dt \tag{14}$$

$$\ddot{\beta} = (\mu_D/I_G)\dot{\delta} - k_{GBH}(1/I_{BH} + 1/I_G)\sin(\beta) + (\mu_W/I_G)\dot{\psi} - (\mu_W/I_G)\dot{\theta} + (1/I_G)T_W + (1/I_G)T_D \tag{15}$$

$$\dot{\psi} = \int\ddot{\psi}\,dt \tag{16}$$

$$\ddot{\psi} = -(\mu_D/I_G)\dot{\delta} + (k_{GBH}/I_G)\sin(\beta) - (\mu_W/I_G)\dot{\psi} + (\mu_W/I_G)\dot{\theta} - (1/I_G)T_D - (1/I_G)T_W \tag{17}$$

$$\dot{\theta} = \int\ddot{\theta}\,dt \tag{18}$$

$$\ddot{\theta} = (\mu_W/I_W)\dot{\psi} - (\mu_W/I_W)\dot{\theta} + (1/I_W)T_W \tag{19}$$

The linear differential equations of motion for the elevation axis are given in Eqs. (20) and (21) of the next section, where ϕ is the elevation angle and $\dot{\phi}$ is the time rate of change of that angle. The torques that are assumed to act on the system are 1) the torque due to the dual elevation drive motors T_E, and 2) a friction torque T_F, which is proportional to the relative angular velocity between the gondola and instrument package. This relative angular velocity is identical to the elevation angle rate, since the gondola is assumed to hang directly beneath the balloon envelope.

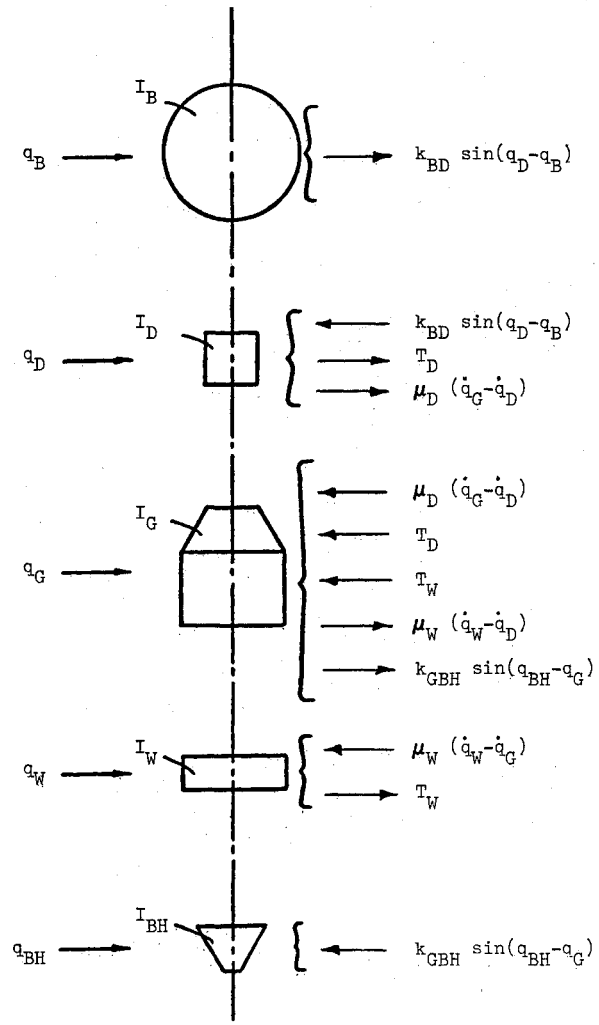

Fig. 2 Torques acting on balloon components.

B. Linear Dynamics

The linear dynamical equations of motion for the balloon and gondola system are written as

$$\dot{\phi} = \int\ddot{\phi}\,dt \tag{20}$$

$$\ddot{\phi} = -(\mu_E/I_E)\dot{\phi} + (1/I_E)T_E \tag{21}$$

$$\dot{\sigma} = \int\ddot{\sigma}\,dt \tag{22}$$

$$\ddot{\sigma} = -k_{BD}(1/I_B + 1/I_D)\sigma + (\mu_D/I_D)\dot{\delta} + (1/I_D)T_D \tag{23}$$

$$\ddot{\delta} = (k_{BD}/I_D)\sigma - (1/I_D + 1/I_G)\dot{\delta} + (k_{GBH}/I_G)\beta - (\mu_W/I_G)\dot{\psi} + (\mu_W/I_G)\dot{\theta} - (1/I_G + 1/I_D)T_D - (1/I_G)T_W \tag{24}$$

$$\dot{\beta} = \int\ddot{\beta}\,dt \tag{25}$$

$$\ddot{\beta} = -k_{GBH}(1/I_{BH} + 1/I_G)\beta + (\mu_D/I_G)\dot{\delta} - (\mu_W/I_G)\dot{\theta} + (\mu_W/I_G)\dot{\psi} + (1/I_G)T_D + (1/I_G)T_W \tag{26}$$

$$\dot{\psi} = \int\ddot{\psi}\,dt \tag{27}$$

$$\ddot{\psi} = -(\mu_D/I_G)\dot{\delta} + (k_{GBH}/I_G)\beta - (\mu_W/I_G)\dot{\psi} + (\mu_W/I_G)\dot{\theta} - (1/I_G)T_W - (1/I_G)T_D \tag{28}$$

$$\ddot{\theta} = (\mu_W/I_W)\dot{\psi} - (\mu_W/I_W)\dot{\theta} + (1/I_W)T_W \tag{29}$$

where all of the variables have previously been defined in Sec. A. The preceding dynamics have been used in the design of the balloon pointing control system with k_{BD} and k_{GBH} set to infinity. These assumptions imply that the balloon/parachute combination acts as a rigid body (i.e., $\sigma = 0$ and $\dot{\delta} = \dot{\psi}$) and that the gondola/ballast hopper connection does not allow any relative motion (i.e., $\beta = 0$). The dynamic coupling between the balloon and the payload gondola is evident from the azimuth rate differential equation, which is a function of $\dot{\delta}$, and therefore, σ and $\dot{\sigma}$.

The dc electrical motors used to provide the control torques can be modeled simply in terms of a motor constant relating the output torque to the input current and a differential equation relating current output to the input voltage. These equations can be written symbolically as

$$T_i = K_i i_i \tag{30}$$

$$\frac{\mathrm{d}}{\mathrm{d}t}(i_i) = -(K_{bi}/L_i)\omega_i - (R_i/L_i)i_i + (1/L_i)u_i \tag{31}$$

where i is replaced by E, D, or W, depending on which motor is being discussed, and u_i represents the voltage control input to the respective motor. Also, K_i is the motor constant, R_i the motor winding resistance, L_i the motor inductance, and K_{bi} the back emf constant of the motor winding. The state variable ω_i in Eq. (31) represents the speed of the ith motor, where i is E, D, or W. For control design purposes, it is assumed that ω_i is $\dot{\phi}$, $-\dot{\psi}$, or $\dot{\theta}$, for i replaced with E, D, or W, respectively.

III. State Space Formulation and LQR Synthesis

A. State Spaces for LQR Controller Synthesis

A general characteristic of control systems is that of driving some steady-state tracking error to zero. It is also generally considered desirable that the zero steady-state tracking error be insensitive to system parameter variations. For these reasons, the system tracking errors are natural state variables for the LQR synthesis procedure.[2,3] The three tracking errors in the balloon pointing control system design are

$$E_\theta = \dot{\theta}_C - \dot{\theta} \tag{32}$$

$$E_\psi = \psi_C - \psi \tag{33}$$

$$E_\phi = \phi_C - \phi \tag{34}$$

where the variables with C subscripts are constant step input commands, and the state variables without subscripts are measured feedbacks. The differential equations for the tracking error states can be written as

$$\dot{E}_\theta = -\ddot{\theta} \tag{35}$$

$$\dot{E}_\psi = -\dot{\psi} \tag{36}$$

$$\dot{E}_\phi = -\dot{\phi} \tag{37}$$

The state space used with the LQR synthesis procedure is now determined separately for each control loop. First consider the elevation angle control problem. For control system design purposes, the elevation behavior is assumed to be dymamically uncoupled from the rest of the vehicle dynamics and is formulated as a SISO control loop. However, the elevation angle control loop must be able to accommodate such unmodeled effects as pendulous coupling between the azimuth and elevation axes and/or wind disturbances. A consistent state space can be formed if Eq. (37) is combined with Eqs. (21), (30), and (31). This state space is controllable and does not include any input command dependent terms, and all of the states and controls are zero in steady state for step input commands. This state space is, therefore, suitable for LQR synthesis. The pointing performance of a controller based upon this state space representation may be inadequate, however, because of unmodeled dynamics such as pendulous swinging of the gondola. This can be interpreted from an LQR synthesis perspective as states and/or controls with nonzero steady-state values (e.g., i_E). A linear controller based on this state space is equivalent to a proportional-derivative positional controller in classical control analysis. Improved elevation pointing performance is likely with the addition of an integrator state, such that proportional-integral-derivative (PID) compensation is employed. This is accomplished with LQR synthesis by combining Eq. (37) with the time derivatives of Eqs. (37), (21), (30), and (31). These equations can be written in the matrix form $\dot{x} = Ax + Bv$ as

$$\begin{bmatrix} \dot{E}_\phi \\ \ddot{E}_\phi \\ \frac{\mathrm{d}}{\mathrm{d}t}(\ddot{\phi}) \\ \frac{\mathrm{d}^2}{\mathrm{d}t^2}(i_E) \end{bmatrix} = \begin{bmatrix} 0 & 1 & 0 & 0 \\ 0 & 0 & -1 & 0 \\ 0 & 0 & -(g\mu_E/I_E) & (gK_E/I_E) \\ 0 & 0 & -(K_{bE}/L_E) & -(R_E/L_E) \end{bmatrix} \begin{bmatrix} E_\phi \\ \dot{E}_\phi \\ \ddot{\phi} \\ \frac{\mathrm{d}}{\mathrm{d}t}(i_E) \end{bmatrix} + \begin{bmatrix} 0 \\ 0 \\ 0 \\ (1/L_E) \end{bmatrix} \dot{u}_E \tag{38}$$

where the state space is $x^T = [E_\phi, \dot{E}_\phi, \ddot{\phi}, \mathrm{d}/\mathrm{d}t(i_E)]^T$, and the scalar control variable is $v = \dot{u}_E$. The states and controls are all zero in steady state in this case even if the motor current is piecewise constant. Again, the state space is controllable, and there are no input command dependent terms in the state space representation. This state space satisfies the requirements outlined in Refs. 2 and 3 and produces an LQR controller with PID compensation, such that zero steady-state tracking is attained even in the presence of the possible model uncertainties. Integral compensation results from the fact that the controller is mechanized with the integral of the state space, but with the gains determined via LQR synthesis on Eq. (38). This mechanization is required to provide the proper motor input of voltage (rather than voltage rate), and the motor input integration cancels the differentiation required to produce the LQR state space with integral compensation. Also, the derivative compensation is implemented as a gain operating on rate feedback.

A backup (failed flywheel) azimuth angle controller state space can be determined in a manner analogous to that of the elevation angle loop. Because of the simplified azimuth axis dynamics (see Sec. II.B) used for control design purposes, the azimuth angle controller must be able to cope with the nonrigid nature of the balloon/parachute suspension, as well as the nonrigid connection between the gondola and the ballast hopper. Furthermore, the azimuth loops must also be able to handle other unmodeled effects such as pendulous coupling between the azimuth and elevation axes and/or wind disturbances. First, Eq. (36) is combined with the time derivatives of

Eqs. (36), (28), (30), and (31) to form a consistent state space. This state space is then determined to be acceptable for the LQR synthesis procedure, since there are no input command dependent terms, and all of the states and controls are zero in steady state for step input commands. The azimuth angle controller design state space that results from the use of just the decoupler motor is written in matrix form as

$$\begin{bmatrix} \dot{E}_\psi \\ \ddot{E}_\psi \\ \frac{d}{dt}(\ddot{\psi}) \\ \frac{d^2}{dt^2}(i_D) \end{bmatrix} = \begin{bmatrix} 0 & 1 & 0 & 0 \\ 0 & 0 & -1 & 0 \\ 0 & 0 & -(g\mu_D/I_G) & -(gK_D/I_G) \\ 0 & 0 & (K_{bD}/L_D) & -(R_D/L_D) \end{bmatrix} \begin{bmatrix} E_\psi \\ \dot{E}_\psi \\ \ddot{\psi} \\ \frac{d}{dt}(i_D) \end{bmatrix} + \begin{bmatrix} 0 \\ 0 \\ 0 \\ (1/L_D) \end{bmatrix} \dot{u}_D \tag{39}$$

which will also produce PID compensation in the LQR design process. The integrator is included to account for the previously discussed model uncertainties. The derivative compensation is again mechanized as a gain in a rate feedback loop. The state space here is $x^T=[E_\psi,\ \dot{E}_\psi,\ \ddot{\psi},\ \mathrm{d}/\mathrm{d}t(i_D)]^T$, whereas the scalar control is $v=\dot{u}_D$.

The full-up azimuth angle state space for MIMO LQR synthesis is more complicated, but can be determined in a manner similar to that used for the SISO control loops. Equation (35) is first equated with the negative of Eq. (29), and then Eqs. (36) and (28), and the D and W subscripted versions of Eqs. (30) and (31) are combined to form a consistent state space where $\dot{\theta}$ is replaced with $E_{\dot{\theta}}$ by adding and subtracting appropriate terms in $\dot{\theta}_C$. Input command dependent terms appear in this state space representation, and all of the states and controls (e.g., i_W and u_W) do not generally have zero steady-state values. For these reasons Eqs. (36), (28), and (29), and the D and W subscripted versions of Eqs. (30) and (31), are differentiated and combined with Eqs. (35) and (36) to form a new state space that is controllable, consistent, has no input command dependent terms, and has zero steady-state values for all state and control variables. The controllability of the MIMO state space must be evaluated after the addition of the integrator states to avoid the introduction of uncontrollable modes.[3] This LQR synthesis compatible state space can be written in the matrix form of $\dot{x}=Ax+Bv$ where the control matrix is $v^T=[\dot{u}_W,\ \dot{u}_D]^T$ and the state space is $x^T=[E_{\dot{\theta}},\ \ddot{\theta},\ E_\psi,\ \dot{E}_\psi,\ \ddot{\psi},\ \mathrm{d}/\mathrm{d}t(i_W),\ \mathrm{d}/\mathrm{d}t(i_D)]^T$. The system matrices are given by

$$A = \begin{bmatrix} 0 & -1 & 0 & 0 & 0 & 0 & 0 \\ 0 & -\frac{g\mu_W}{I_W} & 0 & 0 & \frac{g\mu_W}{I_W} & \frac{gK_W}{I_W} & 0 \\ 0 & 0 & 0 & 1 & 0 & 0 & 0 \\ 0 & 0 & 0 & 0 & -1 & 0 & 0 \\ 0 & \frac{g\mu_W}{I_G} & 0 & 0 & -\frac{g(\mu_W+\mu_D)}{I_G} & -\frac{gK_W}{I_G} & -\frac{gK_D}{I_G} \\ 0 & -\frac{K_{bW}}{L_W} & 0 & 0 & 0 & -\frac{R_W}{L_W} & 0 \\ 0 & 0 & 0 & 0 & \frac{K_{bD}}{L_D} & 0 & -\frac{R_D}{L_D} \end{bmatrix}$$

$$B^T = \begin{bmatrix} 0 & 0 & 0 & 0 & 0 & \frac{1}{L_W} & 0 \\ 0 & 0 & 0 & 0 & 0 & 0 & \frac{1}{L_D} \end{bmatrix}^T \tag{40}$$

This procedure produces a MIMO controller that has a PID structure in the azimuth angle channel and a PI structure in the wheel speed channel. Integral compensation is required in this case to properly decouple the payload gondola from the balloon and to provide good tracking, even for such unmodeled effects as pendulous swinging and wind disturbances. As in the case of the SISO controllers, the derivative feedback of the azimuth angle channel is mechanized as a gain in a rate feedback loop.

B. Linear Quadratic Regulator Procedure

The LQR synthesis problem is that of determining the control that minimizes the performance index

$$J=\int(x^TQx+v^TRv)\,\mathrm{d}t \tag{41}$$

where $R>0$ and $Q\geq 0$, subject to the dynamic constraints

$$\dot{x}=Ax+Bv \tag{42}$$

where the A and B matrices for the balloon control loops are defined symbolically in part A of this section. The solution to this optimization problem is a linear controller of the form

$$v=-(R^{-1}B^TP)x=-Gx \tag{43}$$

where P is the algebraic matrix Riccati equation solution.[7,8] The constant gain matrix, G, can be determined from any of the computer-aided control system design software packages which are currently available to solve the LQR optimization problem. Although the preceding optimization problem is stated in continuous time, the simulation test gains for the balloon are based on determining the discrete form of Eq. (42) and the associated discrete gains for a particular sample rate. Numerical difficulties due to scaling problems are sometimes observed if the fast motor dynamics are included in the state space representation with the relatively slow system dynamics. Although there have been no problems in using the gains determined in such cases, the difficulty is alleviated with little or no performance degradation by removing the motor dynamics from the state space representation.

The various LQR determined compensators are depicted in block diagram form in Figs. 3-5. In each case the motor current state feedbacks have been omitted, since the gains on these states are extremely small and negligible, because of the fast dynamic response of the motors relative to the other system dynamics.

The LQR state weighting matrix for each of the balloon control loops is chosen so as to satisfy several design criteria. In each case, Q is chosen to position the closed-loop system poles such that they provide acceptable transient response behavior, reasonable system bandwidth, and gains that do not produce intolerable noise amplification. Because of the addition of the closed-loop zero in the PID positional control loops, as the weighting on the integrator state [error variable in Eq. (42)] is reduced to zero, the integrator gain approaches zero and the compensation approaches that of a proportional-

derivative controller. This feature simplifies the adjustment of the relative degree of integral compensation. System parameter variation sensitivity is also used to evaluate the choice of each state weighting matrix.

In the case of the MIMO azimuth angle controller, adequate decoupling between the azimuth angle and flywheel speed channels is added to the list of design requirements. This is accomplished with a careful choice of Q, as well as an appropriate choice of R. The state weighting matrix is selected to place maximum emphasis on minimizing the azimuth angle error variables by choosing diagonal weighting elements on the azimuth angle error states which are two and three orders of magnitude, respectively, larger than the wheel speed error state weighting. To reduce nonlinear effects on pointing accuracy, it is also considered desirable that the azimuth angle pointing be accomplished primarily by the flywheel, with the decoupler serving only to uncouple the gondola from the balloon/recovery parachute dynamics. This has been achieved by selecting a diagonal control weighting matrix such that the decoupler motor control weighting is one order of magnitude greater than that of the flywheel motor control weighting.

IV. Singular Value Analysis

The robustness of the LQR balloon control system has been investigated with the use of singular value analysis. Singular value analysis is analogous to the SISO gain and phase margin measures of the closeness of the Nyquist plot to the $(-1,0)$ point in that the measure of this distance for MIMO systems is in terms of the singularity of a matrix. The LQR with a control weighting matrix of the form of an identity matrix multiplied by a scalar has been shown in Refs. 5 and 6 to have useful robustness properties. For a diagonal error model (no coupling between channels), the LQR has simultaneously in each feedback loop a guaranteed minimum gain margin of $(-6,\infty)$ dB and a guaranteed minimum phase margin of ± 60 deg. Since the controls of the MIMO azimuth controller are not equally weighted, a measure of the gain and phase margins of the proposed design is required. The procedures of Ref. 9 are applicable, given the singular values of the return difference matrix

$$D(s)=\left[I+K(s)G_p(s)\right] \tag{44}$$

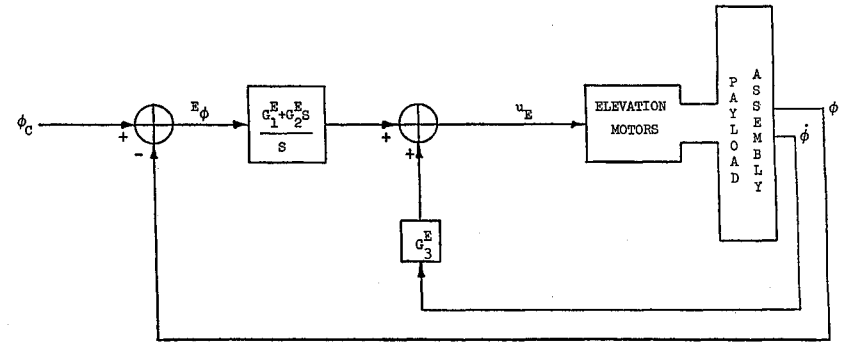

Fig. 3 Elevation angle controller.

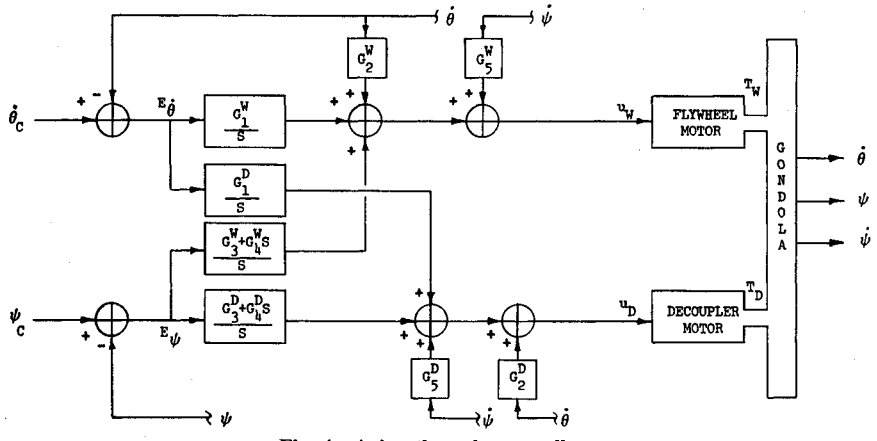

Fig. 4 Azimuth angle controller.

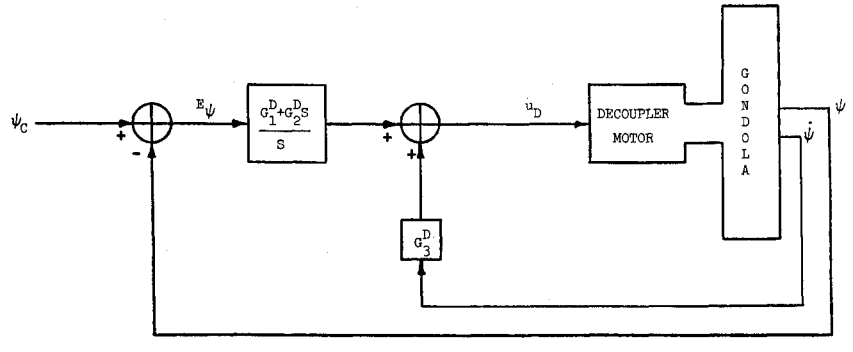

Fig. 5 Decoupler-alone azimuth angle controller.

where $K(s)$ is the compensator transfer matrix and $G_p(s)$ is the plant transfer matrix given by $G_p(s)=C(sI-A)^{-1}B$ such that $K(s)G_p(s)\approx G(sI-A)^{-1}B$. These gain and phase margin results are associated with the nominal system. Singular value analysis can also be useful in assessing the robustness of the system with respect to parameter variations and neglected dynamics. The matrix of most interest here is the inverse return difference matrix

$$T(s)=I+\left[K(s)G_p(s)\right]^{-1} \tag{45}$$

The central robustness relationship[10] (which guarantees that the matrix $T+L$ does not lose rank) is that

$$\underline{\sigma}\left[T(\omega)\right]>\bar{\sigma}\left[L(\omega)\right] \tag{46}$$

for all frequencies ω, where the smallest singular value $\underline{\sigma}$ and the largest singular value $\bar{\sigma}$ are found from the respective square roots of the eigenvalues of the Hermitian matrix $T(-\omega)^TT(\omega)$ or $L(-\omega)^TL(\omega)$. $L(\omega)$ is a multiplicative error model, since, if $G_p(s)$ is the nominal plant, then the perturbed plant G_p^* is expressed as

$$G_p^*=G_p(s)\left[I+L(s)\right] \tag{47}$$

If condition (46) is satisfied, then stability is guaranteed. The condition given by Eq. (46) is conservative, and failure to meet this condition does not necessarily imply system instability. The recent literature[11,12] has described efforts at developing less conservative stability tests.

The construction of the error models is important to evaluate control system robustness. The error models of most concern here are those associated with the important system parameters in the A and B matrices. The error model associated with parameter variations can be derived with the use of a matrix identity. Define $\psi(s)=(sI-A)^{-1}$. A parameter variation can alter both the A and B matrices. These perturbations are denoted here by and ΔA and ΔB, respectively. The perturbed plant is given by

$$G_p^*=C[\psi^{-1}+\Delta A]^{-1}(B-\Delta B)=G_p(I+L_p) \tag{48}$$

With the use of the matrix inversion lemma[10]

$$(\psi^{-1}+\Delta A)^{-1}=\psi-\psi\Delta A(I+\psi\Delta A)^{-1}\psi \tag{49}$$

Eq. (48) becomes

$$G_p^*=C\left[\psi-\psi\Delta A(I+\psi\Delta A)^{-1}\psi\right](B-\Delta B) \tag{50}$$

Since $G_p=C\psi B$, Eq. (48), using Eq. (50), produces

$$\bar{\sigma}(L_p)=\bar{\sigma}\Big(G_p^{-1}C\psi\Big[\Delta B+\Delta A(I+\psi\Delta A)^{-1}\psi B -\Delta A(I+\psi\Delta A)^{-1}\psi\Delta B\Big]\Big) \tag{51}$$

This error model has been used to evaluate the robustness of the balloon LQR controller designs as is discussed in the next section.

V. System Performance

The performance of the balloon payload pointing control system has been evaluated from a singular value analysis and from time response behavior against a dynamic simulation based on Eqs. (11-21) and Eqs. (30) and (31).

Azimuth controller gains and the associated weighting matrices and system eigenvalues are given in Table 2. The elevation axis controller will not be discussed here since performance against the simple linear model of Eqs. (20) and (21) is not particularly instructive.

Representative simulated azimuth axis transient responses are given in Figs. 6–8. The normal azimuth angle controller has been used to produce Figs. 6 and 7, whereas the backup azimuth angle controller has been employed to generate Fig. 8. The transient nature of the MIMO azimuth angle controller is given in Fig. 6 for an azimuth angle command of 10 deg. The corresponding transient response of the flywheel is given in Fig. 7. The flywheel was operating in steady state with an angular velocity of 60 rpm when the step command was input to the azimuth angle controller. The flywheel transient serves to help reorient the gondola, but the flywheel returns to its commanded steady-state angular velocity once the reorientation is complete, since the decoupler has effectively isolated the balloon from the gondola. The decoupler is capable of handling the azimuth pointing of the gondola in the case of a failed flywheel motor as shown in Fig. 8. The transient response performance of the decoupler-alone controller is generally poorer than that obtained from the coordinated use of the flywheel and decoupler, however. In addition to the nominal responses, off-nominal responses due to parameter variation are also shown in Figs. 6–8, with the off-nominal responses labeled by P or M. The parameters of significance are the motor friction coefficients and motor effectiveness constants. These parameters are subject to considerable change due to the harsh upper-atmosphere environment in which the balloon operates. The P transients include parameter variations of $+100\%$ in the friction coefficients and -50% in the motor constants for the MIMO controller. The decoupler motor constant is reduced by only 20% in the P transient of the decoupler-alone azimuth controller. The M transients include parameter variations of -100% in the friction coefficients and $+50\%$ in the motor constants. The performance of the MIMO azimuth controller is not seriously degraded by these large parameter variations. The SISO azimuth controller is much more sensitive to parameter variation, particularly to a decrease in the decoupler motor constant. Both controllers are

Table 2 Azimuth control systems

MIMO azimuth controller	
Performance index weights	
Q(1,1) = 1, Q(3,3) = 50, Q(4,4) = 1000, all other elements are zero	
R(1,1) = 1, R(2,2) = 10, all other elements are zero	
Continuous time gains	
0.4931 −0.8570 −6.1516 −68.8725 294.7756 0.0 0.0	
−0.2751 3.8795 −1.1026 −25.8651 308.4734 0.0 0.0	
Sample rate Δt = 0.10 s gains	
0.48 −0.88 −5.97 −67.03 287.56 0.0 0.0	
−0.27 3.86 −1.09 −25.67 307.19 0.0 0.0	
Open-loop S-plane eigenvalues (motor dynamics omitted)	0.0 0.0 0.0 −0.0063 −0.0001
Closed-loop S-plane eigenvalues (motor dynamics omitted)	$-0.2547\pm0.2616i$ $-0.0577\pm0.0769i$ −0.1112
SISO (decoupler only) azimuth controller	
Performance index weights	
Q(1,1) = 2, Q(2,2) = 20, all other elements are zero	
R(1,1) = 1	
Continuous time gains	
−1.4142 −32.2130 359.6423 0.0	
Sample rate Δt = 0.10 s gains	
−1.40 −32.00 358.04 0.0	
Open-loop S-plane eigenvalues (motor dynamics omitted)	0.0 0.0 −0.00008014
Closed-loop S-plane eigenvalues (motor dynamics omitted)	−0.0878 $-0.0456\pm0.0770i$

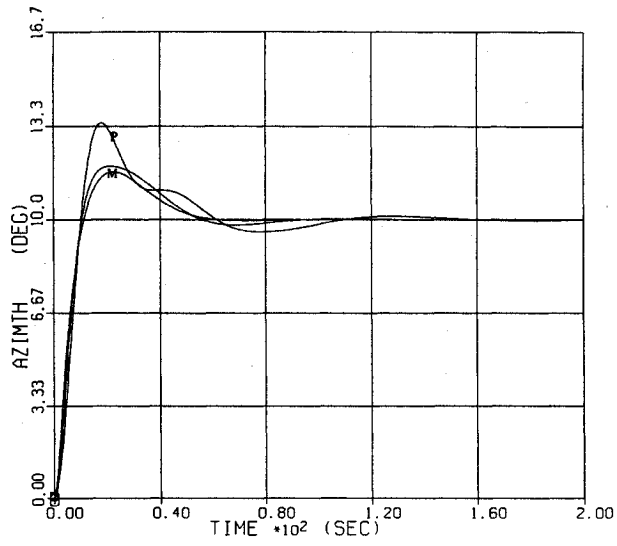

Fig. 6 Azimuth angle pointing of MIMO controller.

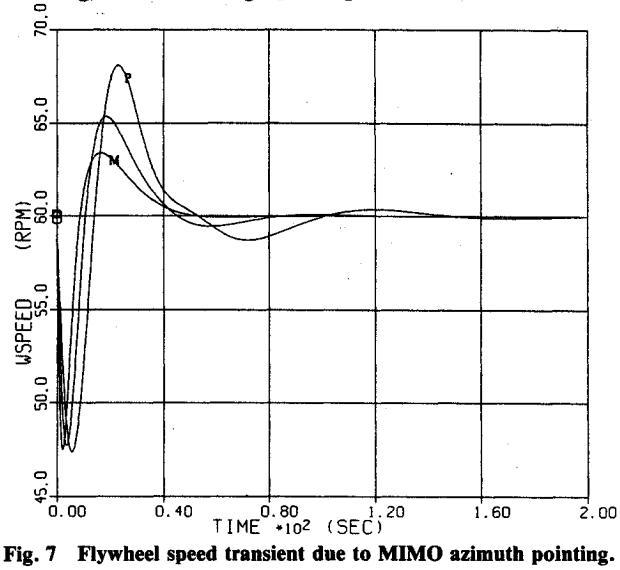

Fig. 7 Flywheel speed transient due to MIMO azimuth pointing.

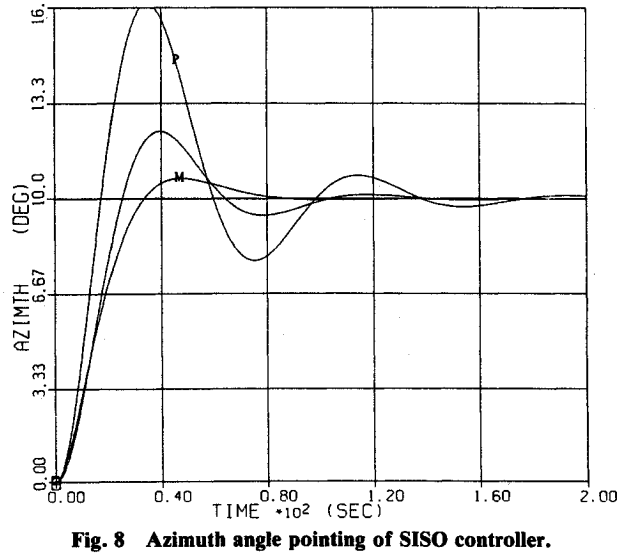

Fig. 8 Azimuth angle pointing of SISO controller.

relatively insensitive to changes in the friction coefficients when compared to similar motor constant variations.

A singular value plot of the return difference matrix [Eq. (44)] is given in Fig. 9. This plot shows a minimum of −0.9 dB. Since an LQR design with equal control weights would

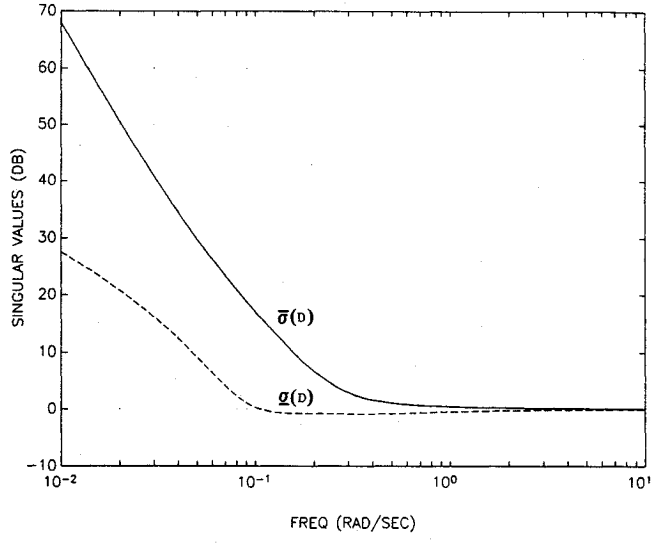

Fig. 9 Singular values of MIMO return difference matrix.

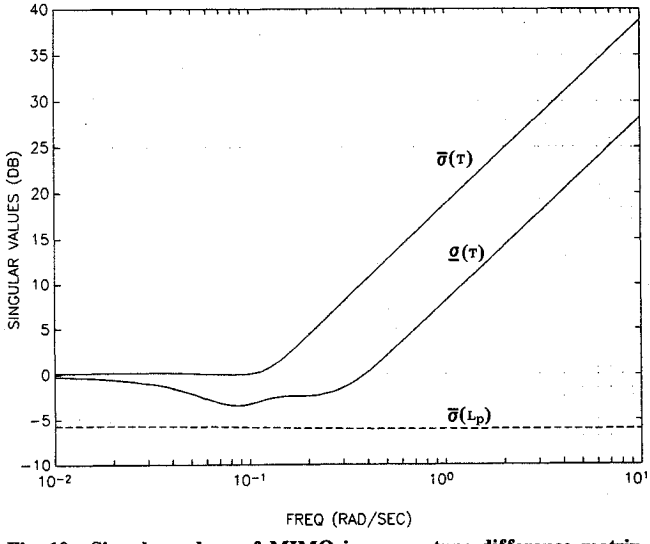

Fig. 10 Singular values of MIMO inverse return difference matrix and parameter variation error model.

have a minimum of 0.0 dB, there is a stability margin penalty in this case for the unequal control weights. The gain and phase margins of this design can be determined from Ref. 9 as a gain margin of (−5, +20) dB and a phase margin of ±53 deg. Figure 10 shows the singular values of the inverse return difference matrix [Eq. (45)] for the MIMO azimuth angle control system plotted against the error model [Eq. (51)] for the parameter variations of +100% in the friction coefficients and −50% in the motor constants. Since $\bar{\sigma}(L_p) < \underline{\sigma}(T)$ for all frequencies, stability is guaranteed. Although the plots are not shown, individual parameter variations confirm that the controller is more sensitive to changes in the motor constants than in the friction coefficients. Similar parameter sensitivity studies have also been used to evaluate the robustness of the SISO systems.

VI. Conclusions

The application of linear-quadratic-regulator (LQR) theory to the design of a pointing control system for a high-altitude research balloon payload is described. This approach is motivated by the multiple-input/multiple-output (MIMO) nature of the azimuth axis pointing problem. The choice of the state space upon which the LQR synthesis is to be applied is analogous to the selection of the compensator structure in classical control theory. The state spaces are selected to ensure zero

steady-state tracking for parameter variation and modeling uncertainty by the addition of states which are equivalent to the addition of integrators to the compensator. The resulting state spaces are consistent and controllable with each of the state variables zero in steady state. The controllability of the MIMO state space is verified after the addition of the integrator states to avoid the introduction of uncontrollable modes.

The choice of the weighting matrices in the LQR performance index is analogous to the choice of gains in a classical approach. The bandwidth of the system and relative speed of the system modes are adjusted (within the constraints imposed by LQR synthesis) for acceptable performance via systematic adjustments of the weights. To provide improved decoupling, the controls of the MIMO azimuth angle controller are not weighted equally.

The robustness of the control system design is investigated with a singular value analysis. Gain and phase margins are determined from the minimum singular value of the return difference matrix. Since the MIMO azimuth controller design does not have equal control weights, these margins are somewhat smaller than the gain and phase margins which are typically assumed for LQR designs. Stability against parameter variation is evaluated with plots of the minimum singular value of the inverse return difference matrix against the maximum singular value of a multiplicative error model. Although this test is conservative, stability is guaranteed for the MIMO azi-muth angle controller for large variations in the important system parameters. The time response behavior of the control system is also tested in a single-degree-of-freedom, simplified nonlinear simulation. The performance of the MIMO azimuth angle controller is not seriously degraded by the introduction of the large, but not destabilizing, parameter variations from the singular value analysis.

The LQR pointing control system design of this paper appears to have the potential for providing the desired pointing accuracy of 0.1 deg or less in azimuth and elevation angle. However, a final assessment would require the use of a more sophisticated simulation or hardware-in-the-loop testing to better quantify the attainable accuracy in the presence of all of the system nonlinearities.

References

[1]Watts, A. C., "Instrumentation for a Balloon-Borne Gamma Ray Astronomy Experiment," *Proceedings of the Ninth AFGL Scientific Balloon Symposium,* Air Force Geophysics Laboratory, Hanscom AFB, MA, Oct. 1976, pp. 215–230.

[2]Athans, M., "On the Design of P-I-D Controllers Using Optimal Linear Regulator Theory," *Automatica,* Vol. 7, Sept. 1971, pp. 643–647.

[3]Speyer, J. L., White, J. E., Douglas, R., and Hull, D. G.,"Multi-Input/Multi-Output Controller Design for Longitudinal Decoupled Aircraft Motion," *Journal of Guidance, Control, and Dynamics,* Vol. 7, No. 6, 1984, pp. 695–702.

[4]Sain, M., (ed.), "Special Issue on Multivariable Control," *IEEE Transactions on Automatic Control,* Vol. AC-26, Feb. 1981.

[5]Safonov, M. G., and Athans, M., "Gain and Phase Margin for Multiloop LQG Regulators," *IEEE Transactions on Automatic Control,* Vol. AC-22, April 1977, pp. 173–179.

[6]Lehtomaki, N., Sandell, N., and Athans, M., "Robustness Results in Linear-Quadratic Gaussian Based Multivariable Control Design," *IEEE Transactions on Automatic Control,* Vol. AC-26, Feb. 1981, pp. 75–92.

[7]Brockett, R., *Finite Dimensional Linear Systems,* Wiley, New York, 1970.

[8]Bryson, A., and Ho, Y.-C., *Applied Optimal Control,* Blaisdell, Waltham, Mass., 1969.

[9]Mukhopadhyay, V., and Newsom, J., "Application of Matrix Singular Value Properties for Evaluating Gain and Phase Margin of Multi-loop Systems," *Proceedings of the AIAA Guidance, Navigation, and Control Conference,* AIAA, New York, 1982, pp. 420–428.

[10]Doyle, J., and Stein, G., "Multivariable Feedback Design: Concepts for a Classical/Modern Synthesis," *IEEE Transactions on Automatic Control,* Vol. AC-26, Feb. 1981, pp. 4–16.

[11]Morton, B. G., "New Applications Of Mu To Real Parameter Variation Problems," *Proceedings of the 24th IEEE Conference On Decision and Control,* Inst. of Electrical and Electronics Engineers, New York, Dec. 1985, pp. 233–238.

[12]de Gaston, R. R. E., and Safonov, M. G., "Exact Calculation of the Multiloop Stability Margin," *IEEE Transactions On Automatic Control,* Vol. AC-33, Feb. 1988, pp. 156–171.